Conference paper

Marcel Miglierini* and Peter Matúš

Structural modifications of metallic glasses followed by techniques of nuclear resonances

DOI 10.1515/pac-2016-1128

Abstract: Iron-based metallic glasses (MGs) are typical representatives of disordered alloys. They exhibit amorphous structure that is lacking any long-range order. Appropriate chemical composition of MGs ensures soft magnetic properties suitable for variety of practical applications. Because the beneficial magnetic properties are closely related to structural features of MGs it is inevitable to understand the ways how and under which conditions is their original structure modified. Notably elevated temperature can induce formation of crystallites that alter the desired magnetic parameters. Here, we demonstrate the use of ^{57}Fe Mössbauer spectrometry and nuclear forward scattering of synchrotron radiation for the study of structural transformations in $(Fe_{2.85}Co_1)_{77}Mo_8Cu_1B_{14}$ MG which was chosen as an example. These techniques are based upon nuclear resonances that can scan evolution of hyperfine interactions acting upon nuclear levels of a stable ^{57}Fe isotope. Because iron is typical constituent element of MGs, any deviations from original structural arrangement including modifications of the chemical surrounding can be studied.

Keywords: hyperfine interactions; metallic glasses; Mössbauer spectrometry; nuclear forward scattering of synchrotron radiation; SSC-2016; structural transformations.

Introduction

Metallic glasses (MGs) have been introduced already couple of decades ago. Namely Fe-based MGs belong to a class of amorphous materials [1, 2] that are still attractive due to their unique magnetic [3] as well as mechanical [4] properties. Because of their excellent magnetic parameters, they can be used as magnetic shielding, sensors or transformer cores [5]. The long-term reliability of their performance under tough conditions with high temperature and in the presence of corrosion agents is an important technologic, economic, and environmental demand, and it raises a number of challenges.

It is noteworthy that selected MGs are used as precursors for preparation of the so-called nanocrystalline alloys which are characterized by a presence of crystalline grains several nanometers in size embedded in a residual amorphous matrix. Such structural arrangement exhibits magnetic parameters superior to those of the original amorphous MGs [3, 6]. There are three main families of nanocrystalline alloys, namely the so-called FINEMET [7], NANOPERM [8], and HITPERM [9] alloys. Recently, nanocrystalline Fe-Si-B-P-Cu soft magnetic alloys called NANOMET [10] with high Fe content have attracted much attention for high performance

Article note: A collection of invited papers based on presentations at the 12th Conference on Solid State Chemistry (SSC-2016), Prague, Czech Republic, 18–23 September 2016.

***Corresponding author: Marcel Miglierini,** Slovak University of Technology in Bratislava, Faculty of Electrical Engineering and Information Technology, Institute of Nuclear and Physical Engineering, Ilkovičova 3, 812 19 Bratislava, Slovakia; and Department of Nuclear Reactors, Czech Technical University in Prague, V Holešovičkách 2, 180 00 Prague, Czech Republic, e-mail: marcel.miglierini@stuba.sk. http://orcid.org/0000-0002-4320-5191
Peter Matúš: Institute of Laboratory Research on Geomaterials, Faculty of Natural Sciences, Comenius University in Bratislava, Ilkovičova 6, 842 15 Bratislava, Slovakia

magnetic applications. Nanocrystalline metallic alloys (NCAs) represent a new class of nanocomposite materials the physical properties of which can be tailored not only by alternating their chemical composition but also by varying the size of crystalline grains, their morphology and structural arrangement. They can be effectively prepared by controlled crystallization of MGs with appropriate compositions. The size of the structural elements (nanocrystals) dominantly influences mechanical, optical, electrical, and/or magnetic properties. Disordered nature of structural arrangement in nanocrystalline alloys gives rise to advantageous (from the point of view of practical application) magnetic properties [11]. Especially, nanocrystalline alloys have attracted a lot of scientific interest because, contrary to their amorphous counterparts, their magnetic parameters do not substantially deteriorate at elevated temperature during practical exploitation. So, it is essential to understand structural behavior of the original amorphous precursors.

Disordered structure of MGs restricts the pool of analytical techniques that are suitable for characterization of their structural arrangement. Indeed, the latter can be studied only indirectly via hyperfine interactions that sensitively reflect the slightest deviations in nuclear levels. Thus, local probe-based methods should be employed. Among them, Mössbauer spectrometry plays an unmatched role namely because of its ability to provide simultaneous information on both structural arrangement and magnetic states of the resonant ^{57}Fe nuclei. Their states are substantial governed by chemical surroundings. Even though the evaluation of Mössbauer spectra of disorder systems is not a trivial task the diagnostic potential of this method proved to be very effective particularly in acquiring new insights into MGs. Structural modifications are reflected via hyperfine interactions that cause shifts and/or splitting of the nuclear levels and can be sensitively recorded by this technique.

Temperature dependent structural transformation in MGs are routinely followed by analytical techniques like X-ray diffraction, differential scanning calorimetry (DSC), transmission electron microscopy or by magnetic measurements. Only few of them, however, is capable of providing *in situ* investigations in real time. The most typical examples comprise DSC and magnetic measurements. Even then, the obtained information cannot unambiguously identify newly formed nanocrystals qualitatively (type of crystals). To fulfill this task, one should consider the use of a less common method that also makes use of nuclear resonances at ^{57}Fe nuclei, namely the so-called nuclear forward scattering (NFS) of synchrotron radiation.

Here, we demonstrate the use of Mössbauer spectrometry and NFS in the investigation of structural transformations that are taking place in Fe-based MGs under the effect of elevated temperature. We have chosen $(Fe_{2.85}Co_1)_{77}Mo_8Cu_1B_{14}$ MG as an example. Both methods utilize ^{57}Fe nuclei as local probes. Before presenting selected case studies, we briefly mention basic aspects of the techniques with a special emphasis on complementarities and distinctions between them.

Mössbauer spectrometry

Mössbauer spectrometry [12] is one of few analytical techniques that can contribute to the description of structural arrangement and its consequences towards magnetic states of such systems that lack any long-range order structural arrangement, i.e. to the study of disordered systems like MGs. In doing so, a possibility to derive distributions rather than unique values of the respective spectral parameters from the Mössbauer spectra is an asset. Electric quadrupole and magnetic dipole hyperfine interactions sensitively reflect any deviations in chemical and/or topological short-range order in these systems. Contrary to for example diffraction techniques, information on the local arrangement from the viewpoint of both structure and magnetic order is simultaneously accessible. Moreover, all structurally different regions are readily recognized within the inspected samples.

Basic features of Mössbauer line assignment are schematically illustrated in Fig. 1 for the case of ^{57}Fe resonant nuclei that are located in non-magnetic or magnetic structural positions within a crystalline or amorphous structure. Crystalline materials (CR) exhibit long-range order translation symmetry over several lattice constants and their Mössbauer spectrum features well-defined narrow lines. Depending upon the hyperfine interactions, the obtained Mössbauer spectrum is doublet and sextet for non-magnetic and magnetic samples,

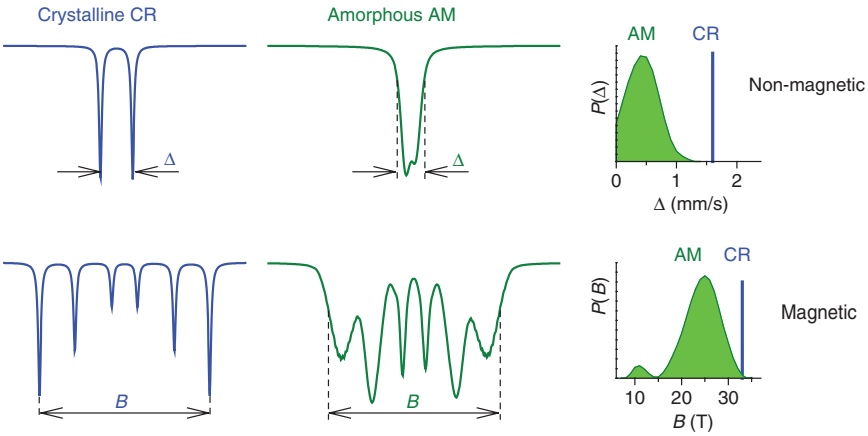

Fig. 1: Model Mössbauer spectra of crystalline (CR) and amorphous (AM) systems with the respective hyperfine spectral parameters (see text).

respectively. The relevant spectral parameters comprise quadrupole splitting Δ and hyperfine magnetic field B, both of them having unique and precisely defined values for a particular Fe site in a crystalline lattice. On the other hand, due to non-equivalent atomic sites in disorder amorphous (AM) systems the corresponding Mössbauer lines are broadened and exhibit distributions of the respective hyperfine parameters $P(\Delta)$ and $P(B)$ as demonstrated at the right-hand side of Fig. 1.

Narrow and broad spectral lines are observed namely in nanocrystalline alloys. While the former belong to nanocrystalline grains the latter are ascribed to the residual amorphous matrix and to the so-called interface regions (i.e. surfaces of the nanograins) [13, 14].

Mössbauer spectrometry provides valuable information on structural (and/or magnetic) arrangement of MGs. Nevertheless, in general it takes hours to record a Mössbauer spectrum with sufficient statistics when laboratory sources of ionizing radiation are employed. Consequently, these studies are limited to static conditions of the investigated system (e.g. temperature, external magnetic field, etc.). In order to follow rapid evolution of structural modifications in real time *in situ* NFS experiments can be considered.

Nuclear forward scattering of synchrotron radiation

With the onset of new generation of synchrotron sources, tuneable energy of synchrotron radiation featuring extremely high brilliance become available [15]. It allows experiments in real time that scan the investigated MG during the influence of the external conditions. The use of synchrotron radiation for on line characterization is often used by diffraction techniques [16–18] that are rather limited in the description of amorphous systems. Recently, more sophisticated techniques of real-time *in situ* synchrotron X-ray tomographic microscopy [19] and combination of time-resolved X-ray photon correlation spectroscopy and high-energy X-ray diffraction [20] were applied.

Still, correlation of hyperfine interactions with structural states of the atoms was not possible. This option has evolved with the availability of the third generation synchrotron sources when the method of nuclear forward scattering of synchrotron radiation [21] became possible. NFS makes use of ^{57}Fe resonant atoms as probes of local magnetic and electronic properties in the investigated samples and provides information on hyperfine interactions similar as Mössbauer spectrometry. Because of high number of photons, the time needed for acquisition of relevant data is short enough to inspect structural transformations in real time during *in situ* annealing of MGs [22–25].

NFS belongs to the family of nuclear resonant scattering processes [26] and can be considered as analog of Mössbauer spectrometry [27]. It is especially useful under extreme conditions including high temperature, pressure, and/or magnetic fields when the space with such an environment is very limited and, hence the

sample can be as small as several tens of micrometers. NFS permits on fly inspection of structural and/or magnetic arrangement that continuously evolves with changing temperature/time. So far, it was successfully applied to different studies in materials research [28].

As schematically depicted in Fig. 2, bunches of accelerated particles (electrons) produce flashes of synchrotron radiation with typical duration of ~50 ps and repetition rate ~200 ns. Their energy is tuned to the requested Mössbauer transition using high resolution monochromator that provides energies of photons within a bandwidth of several meV. The pulse contains wider range of energies than is needed for excitation of available nuclear levels in the studied sample and ensures immediate excitation of all nuclear transitions. Energy separation of nuclear levels due to hyperfine interactions is of the order of several hundreds of neV. Thus, all transitions are excited simultaneously at the same time during an impingement of the synchrotron radiation pulse upon the sample.

In time period between two subsequent pulses, all excited nuclei emit the excess energy in a form of resonance delayed photons. All de-excitation photons sum up and give rise to interference patterns in time domain the so-called NFS time-domain patterns as schematically shown in Fig. 3.

Let us remind that in Mössbauer spectrometry, nuclear transitions are excited sequentially one by one as the energy of photons varies over specific values. This is ensured by a transducer which carries the Mössbauer radioactive source and the energy of outgoing photons is modulated due to the Doppler principle. The resulting Mössbauer spectrum is recorded as a function of the Doppler velocity in energy domain.

The counts of delayed photons are registered as a function of time that has elapsed after the excitation. That is why NFS is sometimes referred to as Mössbauer spectrometry in time domain. Single transition is characterized by an exponentially decaying signal (linear in semi logarithmic scale). Multiple photons originating from multiple transitions exhibit characteristic beating of intensities called quantum beats. Their character is unique for particular hyperfine interactions as demonstrated in Fig. 3 for electric quadrupole (non-magnetic) and magnetic dipole interactions, respectively. They carry information on hyperfine interactions that are unique for individual atomic sites of the resonant atoms.

Evaluation of experimental NFS data is performed by their fit to a suitably chosen theoretically calculated model. Each model consists of several sets of hyperfine parameters that are each ascribed to one particular atomic site. The obtained resulting parameters identify valence states, symmetry of charge distribution and magnetic ordering. Phase composition of the material under study can be identified and relative amount of

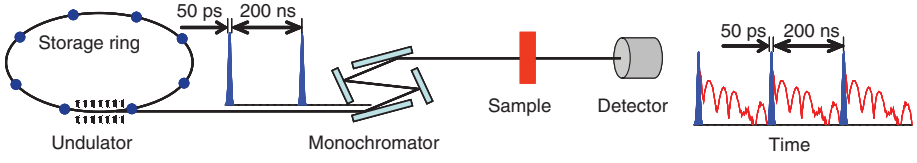

Fig. 2: Basic layout of a typical NFS beamline with the major components.

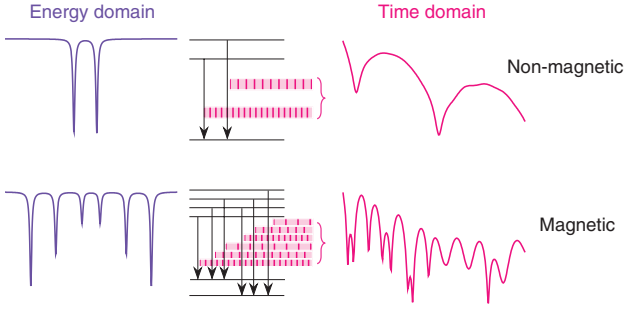

Fig. 3: Mössbauer spectra (left) are obtained in energy domain by sequential recording of nuclear transitions among split nuclear levels (middle). The latter are simultaneously excited by a single pulse of incident synchrotron radiation. Subsequent instantaneous de-excitation provides scattered photons of different energies that sum up to a NFS time-domain pattern (right).

each phase can be determined. Due to high site selectivity we can study local electronic arrangement and its fine distortions can be revealed. We can also study magnetization of individual magnetic structures via hyperfine magnetic fields within magnetically active materials.

Experimental details

Amorphous $(^{57}Fe_{2.85}Co_1)_{77}Mo_8Cu_1B_{14}$ metallic glass was prepared by the method of rapid quenching of a melt upon rotating wheel in a form of ribbons. The casting was done in the air, i.e. no protective atmosphere was used. The width and the thickness of the ribbons were of about 1–2 mm and ~ 20 μm, respectively. Annealing of the original as-quenched alloys was performed at temperatures of up to 550 °C for 30 min in a vacuum. In this way, production of different amounts of nanocrystallites was ensured.

Structural characterization of as-quenched and annealed ribbons was accomplished by the techniques of Mössbauer spectrometry that are sensitive particularly to subsurface regions. Namely, we have employed conversion electron Mössbauer spectrometry (CEMS) and conversion X-ray Mössbauer spectrometry (CXMS). They provide information from the depths of ~ 200 nm and ~ 5–10 μm, respectively. Our samples were produced from iron enriched to about 50 % in the ^{57}Fe isotope. These samples were used to facilitate CEMS, CXMS, and NFS experiments, i.e. to increase the count rate and so to shorten the acquisition time. Chemical composition of the produced ribbons was checked by optical emission spectrometry with inductively coupled plasma (Mo, B) and flame atomic absorption spectrometry (Fe, Co, Cu).

Mössbauer effect experiments were performed at room temperature with a constant acceleration spectrometer using a $^{57}Co/Rh$ source. Calibration was done using a thin (12.5 μm) α-Fe foil. Evaluation of the spectra was accomplished by the Confit software [29]. The obtained isomer shift values are quoted with respect to a room temperature Mössbauer spectrum of a calibration α-Fe foil.

NFS experiments were performed at the Nuclear Resonance side-station ID22N of the European Synchrotron Radiation Facility (ESRF), Grenoble. Excitation of the ^{57}Fe nuclear levels was accomplished by a photon beam with 14.413 keV energy and ~ 3 meV bandwidth. Samples were placed in a vacuum furnace and heated up with a ramping rate of 10 K/min up to 700 °C. The NFS time-domain patterns were continuously recorded every minute during the whole annealing process in transmission geometry. Thus, information on the bulk of the sample was obtained. Evaluation of the experimental NFS data was accomplished by the CONUSS software package [30, 31]. Typically, several tens (up to ~ 140) of time-domain patterns were obtained during one experiment. In order to process and subsequently evaluate such enormous data quantities special software called Hubert was employed which enables sequential fitting procedure [32, 33].

Results and discussion

Mössbauer spectrometry

Using surface sensitive techniques of Mössbauer spectrometry, viz. CEMS and CXMS subtle differences between both surfaces of the annealed ribbons can be unveiled. CEMS and CXMS spectra recorded from air sides of the $(Fe_{2.85}Co_1)_{77}Mo_8Cu_1B_{14}$ ribbons are depicted in Fig. 4. In the as-quenched state (a.q.), broad spectral lines characteristic for magnetically active MG are observed. They were reconstructed by distributions of hyperfine magnetic fields. After moderate annealing at 370 °C, structural relaxation of the amorphous structure has occurred. This is demonstrated by presence of non-magnetic regions that were fitted by distributions of quadrupole splitting. At the same time, bcc-Fe,Co nanocrystallites start to emerge in close-to-surface regions as evidenced by the CEMS spectrum. In more deep subsurface layers, only traces of the corresponding spectral component are identified by CXMS. It is noteworthy that presence of magnetic oxides, most prob-

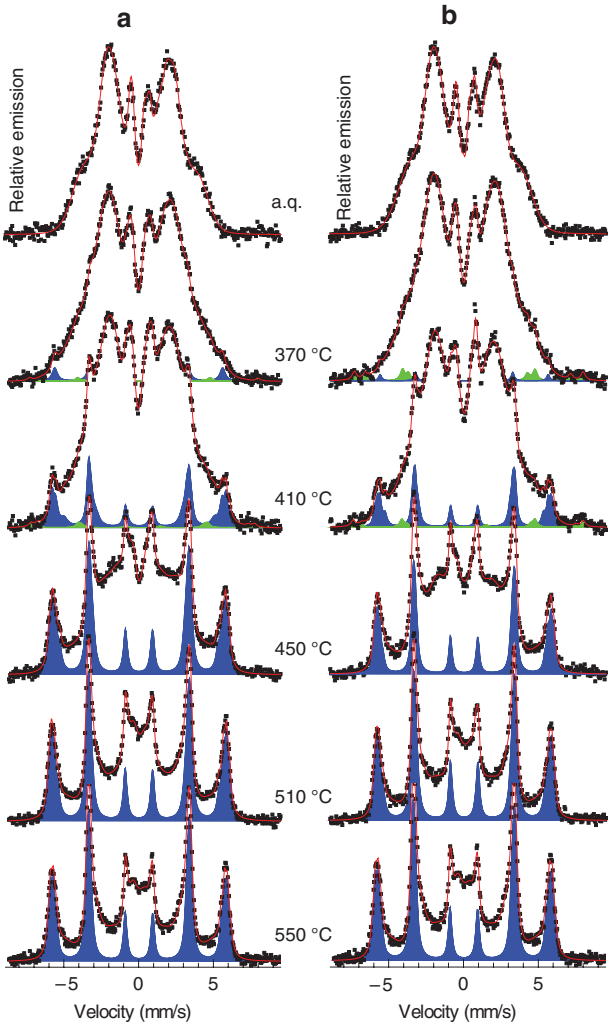

Fig. 4: CEMS (a) and CXMS (b) spectra of the $(Fe_{2.85}Co_1)_{77}Mo_8Cu_1B_{14}$ MG taken from the air sides of ribbons annealed at the indicated temperatures (a.q. = as-quenched). Mössbauer spectral lines corresponding to crystalline phases are plotted in blue (bcc-Fe,Co) and green (Fe oxides).

ably magnetite and/or maghemite is evidenced by occurrence of two sextets. Their content is, however at the detection limit of Mössbauer spectrometry and corresponding spectral parameters are not well defined.

With increasing temperature of annealing, presence of crystalline phases is better documented by well resolved narrow magnetically split spectral components. They correspond to Fe crystallites with bcc structural arrangement whose positions are partially substituted by Co. These parts of the Mössbauer spectra were fitted with a sum of up to four sextets of Lorentzian lines with average hyperfine magnetic fields of 33.4 ± 0.2 T, 35.0 ± 0.1 T, 36.3 ± 0.1 T, and 37.4 ± 0.2 T that can be assigned to Fe atoms in bcc lattice with 1–4 Co atoms in the nearest neighborhood sites. Due to complexity of the master alloy which contains also other chemical elements like Mo and B, contribution of these constituent atoms in the first neighborhood shell cannot be excluded. The obtained hyperfine magnetic fields are affected also by contributions from the second (and possibly higher) shells that are also occupied by foreign Co and Mo atoms. Isomer shift values of the particular sextets are from the range ~0.02–0.06 mm/s (±0.02 mm/s) and their relative areas follow binomial distribution as expected for such structural arrangement.

Room temperature CEMS and CXMS Mössbauer spectra taken from the wheel sides of the as-quenched and annealed $(Fe_{2.85}Co_1)_{77}Mo_8Cu_1B_{14}$ MG are plotted in Fig. 5. From a qualitative point of view, they are similar to those recorded from the air sides (Fig. 4). There are subtle deviations observed in the determined average

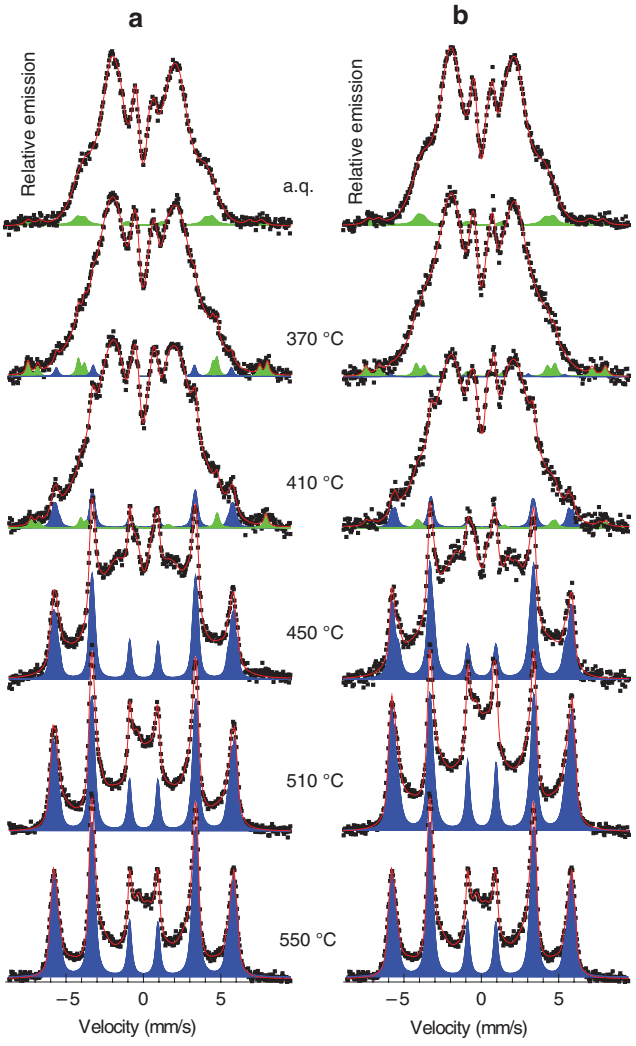

Fig. 5: CEMS (a) and CXMS (b) spectra of the $(Fe_{2.85}Co_{1.77})Mo_8Cu_1B_{14}$ MG taken from the wheel sides of ribbons annealed at the indicated temperatures (a.q. = as-quenched). Mössbauer spectral lines corresponding to crystalline phases are plotted in blue (bcc-Fe,Co) and green (Fe oxides).

values of hyperfine magnetic fields that belong to the particular sextets of the bcc-Fe,Co crystalline phase. Nevertheless, the obtained values of 33.7 ± 0.1 T, 35.1 ± 0.1 T, 36.4 ± 0.1 T, and 37.5 ± 0.1 T fall into the range of experimental errors.

Distinctions between the two sides of the MG ribbons are better documented by the help of Fig. 6 where relative areas of all spectral components are plotted against the temperature of annealing. As seen from Fig. 6a and b, more abundant Fe oxides are detected on the wheel side. They are found already in the as-quenched state and gradually diminish with rising temperature of annealing. They extend also to deeper surface regions because CEMS and CXMS results are almost equal. On the air side, even though some Fe oxides are detected their amount is just at the edge of a detection limit (~1%) of Mössbauer spectrometry. Therefore, no conclusions could be suggested with respect to their origin.

Concerning the presence of Fe oxides on the wheel side, they belong to corrosion products. During the production process, some humid air is trapped between the melt and the quenching wheel. The humidity immediately evaporates and forms air pockets inside which corrosion might be initiated. With increasing temperature of annealing formation of bcc-Fe,Co nanocrystals progresses more rapidly and the resulting Mössbauer spectral lines cover the weak signal from Fe oxides. Even though present, it cannot be detected. It

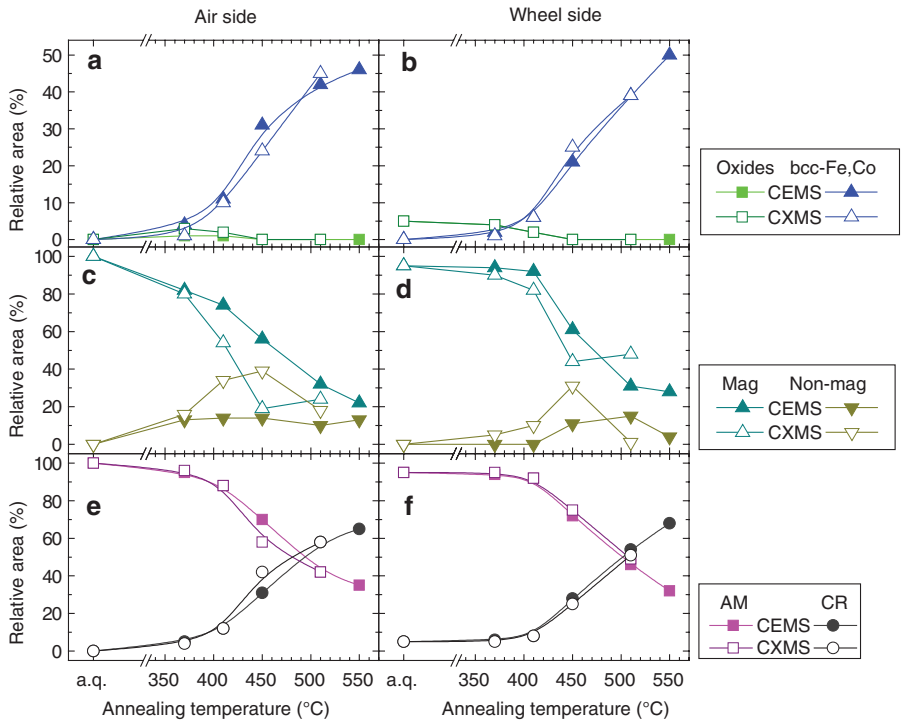

Fig. 6: Relative areas of the corresponding spectral components as derived from CEMS (full symbols) and CXMS (open symbols) spectra of the $(Fe_{2.85}Co_{1})_{77}Mo_{8}Cu_{1}B_{14}$ MG taken from the air (a, c, e) and wheel (b, d, f) sides of the ribbons plotted against temperature of annealing (a.q. = as-quenched).

is noteworthy that the identification of these oxides was possible due to high enrichment of the investigated sample to the ^{57}Fe isotope which is not routinely used for production of MG.

Presence of bcc-Fe,Co nanocrystals is revealed already after moderate annealing at 370 °C and evolves more rapidly on the air side than on the wheel side (Fig. 6a and b). It also starts earlier in the uppermost surface films (CEMS – Fig. 6a). The air side has faced the surrounding atmosphere (air) during the production of the ribbons while the wheel side was in direct contact with the rotating wheel and thus was exposed to better quenching conditions featuring more effective dissipation of heat. Toward high annealing temperatures, the content of detected bcc-Fe,Co phase is similar. Perhaps more crystallites are formed at the surface of the wheel side when the highest annealing temperature is applied.

Particular features of Mössbauer spectrometry are demonstrated in Fig. 6c and d where relative fractions of the residual amorphous matrix are plotted against temperature of annealing. The obtained Mössbauer spectra were fitted using distributions of hyperfine magnetic fields and distributions of quadrupole splitting. As schematically shown in Fig. 1, they correspond to magnetic and non-magnetic regions, respectively, that are found inside the amorphous matrix. So, even though the Mössbauer spectra are broad they can be decomposed into these two components and provide closer insight into hyperfine interactions in the amorphous structure. At low temperatures of annealing, magnetically active regions prevail namely in the close-to-surface regions as evidenced by the CEMS data. Their diminution is continuous on the air side and rather abrupt on the wheel side. Formation of non-magnetic regions can be associated with the development of bcc-Fe,Co nanocrystals. This process, in turn, lowers the amount of magnetic Co and Fe atoms in the residual amorphous matrix and thus enhances contribution of non-magnetic amorphous regions. With growing number of bcc-Fe,Co grains which feature considerable magnetic moments, the overall amorphous matrix is polarized by ferromagnetic exchange interactions among the nanocrystals. Consequently, electric quadrupole hyperfine interactions are suppressed and so is the relative contribution of the non-magnetic spectral component.

Evolution of the amorphous (AM) and overall crystalline (CR) contributions in the annealed $(Fe_{2.85}Co_1)_{77}Mo_8Cu_1B_{14}$ MG is shown in Fig. 6e and f as a function of temperature of annealing. We can conclude that the progress of crystallization is more rapid on the air side of the ribbons where the 50 : 50 ratio is reached after annealing at ~490 °C. On the wheel side, equal contribution from AM and CR components is observed after annealing at a temperature higher by about 20°.

Nuclear forward scattering of synchrotron radiation

Mössbauer effect experiments discussed above provide valuable information about structural and magnetic arrangement of the investigated $(Fe_{2.85}Co_1)_{77}Mo_8Cu_1B_{14}$ MG. Nevertheless, even though specific details on namely amorphous residual phase were achieved that are hidden for majority of other analytical techniques the experiments were accomplished under static conditions. Acquisition of a single CEMS or CXMS spectrum took several tens of hours even though isotopically enriched samples were used. In order to follow structural evolution under dynamically changing conditions we have employed synchrotron radiation using the NFS technique.

Similar as Mössbauer spectrometry also NFS scans hyperfine interactions of the ^{57}Fe resonant nuclei. Contrary to the surface sensitive CEMS and CXMS techniques, the recorded information is obtained from the bulk of the investigated material. Because hyperfine interactions are governed by local atomic order, details on both structural arrangement and magnetic ordering can be obtained simultaneously from NFS time-domain patterns. The latter represent plots of the number of 'delayed' photons, which are emitted by the sample during the process of its de-excitation, as a function of delayed time that has elapsed after the excitation with a synchrotron-radiation pulse.

Selected examples of NFS time-domain patterns are presented in Fig. 7. Experimental data (full symbols) acquired at the indicated temperatures of measurements were fitted with theoretical models and the resulting curves are plotted by red lines. We have chosen typical examples that demonstrate evolution of the patterns in the vicinity of magnetic ordering and structural transitions. Because of qualitative changes in the shapes of the patterns that reflect modifications of the structural arrangement several fitting models were introduced.

According to the Mössbauer effect results, the as-quenched $(Fe_{2.85}Co_1)_{77}Mo_8Cu_1B_{14}$ MG is amorphous and exhibits magnetic interactions. The corresponding physical model consisted of two distributions of hyperfine magnetic fields. Up to ~107 °C, quantum beats assigned to hyperfine magnetic interactions are quite well visible. They are demonstrated by small periodic oscillations in the 35–65 ns time region. Traces of these

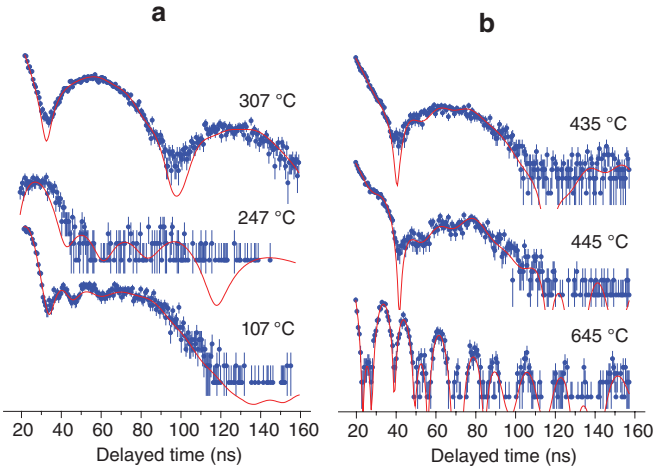

Fig. 7: Selected NFS time-domain patterns obtained from NFS the $(Fe_{2.85}Co_1)_{77}Mo_8Cu_1B_{14}$ MG at the indicated temperatures in the vicinity of magnetic ordering (a) and structural (b) transitions.

beats continuously vanish until they completely disappear at ~247 °C. This is the Curie point (T_C) of this MG beyond which the alloy is non-magnetic though still fully amorphous.

NFS time-domain pattern taken at 307 °C shows typical beat pattern for non-magnetic material (see also Fig. 3). Experimental data corresponding to this temperature interval were modeled with one distribution of quadrupole splitting. This character of the quantum beats persists, from a qualitative point of view, till the onset of crystallization. Nevertheless, the frequency of oscillations gradually becomes lower as seen for example in the NFS time-domain pattern taken at 435 °C in Fig. 7b.

When the annealing temperature reaches the temperature of the onset of crystallization T_{x1} formation of nanocrystalline bcc-Fe,Co grains starts and magnetic interactions are resumed. They are identified by the corresponding quantum beats as demonstrated for example by the NFS time-domain pattern taken at 445 °C in Fig. 7b. Here, more rapid oscillations, which represent hyperfine magnetic fields, appear in the time region 43–83 ns. Finally, at 645 °C the NFS time-domain pattern clearly shows well developed magnetic structure (see also Fig. 3) which means that the degree of crystallization is significantly high.

Based on the above mentioned observations we can divide the studied temperature region into three intervals. In the first one, which extends from room temperature up to T_C (~247 °C), the investigated $(Fe_{2.85}Co_1)_{77}Mo_8Cu_1B_{14}$ MG is amorphous and magnetic. In the second intermediate temperature region where $T_C < T < T_{x1}$, the studied material is still amorphous but magnetic hyperfine interactions have vanished and the sample is non-magnetic (paramagnetic). In the third temperature region beyond T_{x1} (~435 °C) nanocrystalline state of the investigated MG is well established. Evaluation of the NFS time-domain patterns was accomplished in this region with a model that took into consideration both the presence of residual amorphous matrix in paramagnetic state as well as the newly formed bcc-Fe,Co nanocrystals. The former was fitted with one distribution of quadrupole splitting that was applied actually already in the $T > T_C$ region. The latter were represented by four components with hyperfine magnetic fields (not distributed) whose relative fractions were derived from a binomial distribution of the Co nearest neighbors. As demonstrated in Fig. 7b (645 °C) satisfactory fits were achieved.

Overview of all NFS time-domain patterns is presented in Fig. 8 in a form of contour plot. The vertical axis represents temperature of the investigated sample during acquisition of the NFS experimental data while the delayed time of the scattered resonance photons is given on the horizontal one. Counts of the registered photons (intensities) are color coded in a logarithmic scale. Division of the whole investigated temperature range into the particular intervals is also indicated. Obvious changes in the quality of the NFS time-domain patterns clearly indicate the positions of the transformation temperatures T_C and T_{x1} even without any need for quantitative evaluation of the experimental data.

Nevertheless, in order to determine the transition temperatures more accurately we present in Fig. 9 a plot of relative areas of the amorphous (AM) and crystalline (CR) components versus temperature. Temperature of the onset of crystallization T_{x1} is clearly indicated by abrupt increase in the crystalline component. It is

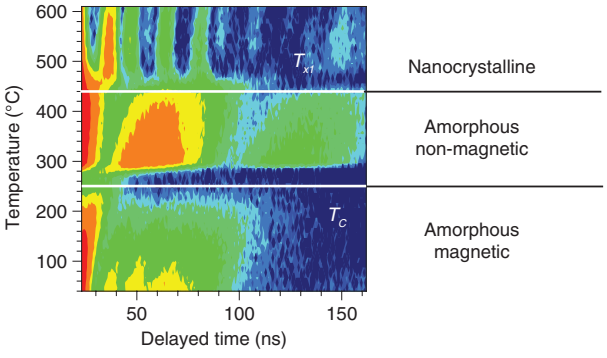

Fig. 8: Contour plot of NFS time-domain patterns recorded from the $(Fe_{2.85}Co_1)_{77}Mo_8Cu_1B_{14}$ MG during *in situ* temperature experiment. Crystallization T_{x1} and Curie T_C temperatures are indicated by the horizontal lines which determine three distinct regions of the MG.

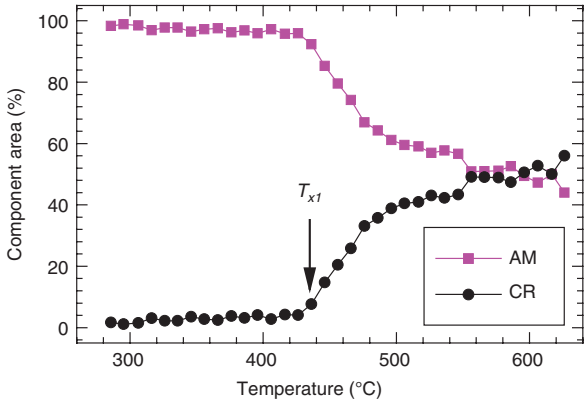

Fig. 9: Relative areas of AM and CR components as derived from NFS time-domain patterns of the $(Fe_{2.85}Co)_{77}Mo_8Cu_1B_{14}$ MG plotted against temperature. Transition temperature T_{x1} is marked with arrow.

noteworthy that crystallization starts in the bulk by about 30–40° later than at the surfaces of the MG ribbons. The same temperature difference is observed also for reaching equal contents of AM and CR phases.

As far as the hyperfine parameters are concerned, average values of magnetic hyperfine fields and quadrupole splitting derived from the amorphous residual matrix of the investigated MG are plotted in Fig. 10 as a function of temperature. Here, huge diagnostic potential of NFS is documented. The first temperature region ($T < T_C$) in Fig. 10a introduces evolution of two hyperfine magnetic fields that were used to fit the NFS time-domain patterns using their distributions. They represent different short-range order arrangements of the resonant ^{57}Fe nuclei in the amorphous structure. The high-field component (~ 22 T at close-to-room temperature) represents Fe neighbors that are surrounded predominantly with Co while the low-field one (~ 8 T) reflects contributions from other constituent elements (Mo, B). Both average magnetic hyperfine fields decrease with temperature as expected. They should vanish at T_C. It should be noted that the low-field component values in the vicinity of T_C (~ 3–5 T) are comparable in strength with the newly developing electric quadrupole interactions and can be hardly distinguished one from another. In this respect, small hyperfine magnetic fields can be treated as quadrupole splitting. On the other hand, the high-field component that attains ~ 11 T at T_C has only marginal relative area at this temperature.

Beyond T_C, the investigated MG is non-magnetic and its amorphous phase is reconstructed by distributions of quadrupole splitting Δ. The obtained average Δ values are plotted in Fig. 10b against the temperature of annealing. Quadrupole splitting provides information about bond properties and local symmetry of the iron sites. Quantitative changes in Δ values at ~ 450 °C coincides with the onset of crystallization. For temperature higher than ~ 500 °C, the newly emerging crystalline phase is already quite well developed and, consequently, also the Δ values are rather stabile.

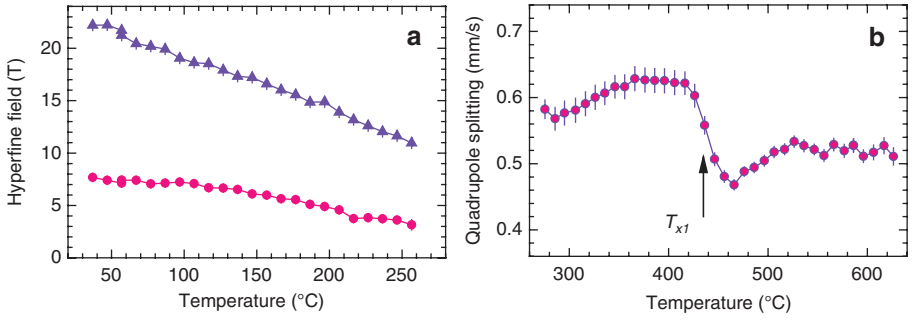

Fig. 10: Average values of hyperfine magnetic fields (a) and quadrupole splitting (b) of the amorphous matrix plotted against the annealing temperature as obtained from the fitting of *in situ* NFS time-domain patterns of the $(Fe_{2.85}Co)_{77}Mo_8Cu_1B_{14}$ MG. Solid lines are only guides to the eye. Transition temperature T_{x1} is marked with arrow.

NFS proved to be suitable technique for providing simultaneous information on both the local structural arrangement and hyperfine interactions. Even though majority of the investigated structure is amorphous, contributions from regions with different chemical short-range order and their evolution can be followed *in situ* as a function of increasing temperature of measurement. Such data can be hardly obtained by another technique. Majority of conventional analytical tools treat amorphous structures as structurally isotropic regions which usually provide only a featureless (broadened and/or halloed) signal.

Conclusions

Modifications of structure of the investigated $(Fe_{2.85}Co_1)_{77}Mo_8Cu_1B_{14}$ metallic glass were followed by employing methods of nuclear resonance. In particular, surface sensitive techniques of Mössbauer spectrometry, viz. CEMS and CXMS were used to unveil subtle differences between the two sides of the metallic glass ribbons. The obtained results have indicated that crystallization process proceeds more rapidly on the air side, i.e. the one which was exposed to the surrounding atmosphere during the production. On the opposite, i.e. the wheel side, which was in direct contact with the quenching wheel, traces of iron oxides were revealed. This was possible due to high isotopic enrichment of the investigated samples to ^{57}Fe nuclei. This has enhanced the sensitivity of the applied surface Mössbauer effect techniques.

Further, we have presented *in situ* NFS experiments that are capable offering unique possibilities for on-fly experiments during continuous variation of for example temperature and thus scan the early stages of crystallization in MGs. This process can be monitored *in situ* starting from formation of nucleation centers, their growth, and continuation towards equilibrium nanocrystalline state. Using this approach, the obtained results are not affected by a cooling process which is the case when *ex situ* Mössbauer effect experiments are employed.

Acknowledgments: Samples of metallic glasses were provided by a courtesy of D. Janičkovič (Bratislava). The authors would like to thank P. Švec (Bratislava), J. Kohout (Prague), and A. Lančok (Husinec-Řež) for their technical assistance during measurements on the synchrotron and V. Procházka and V. Vrba (Olomouc) for their help with NFS data processing. This work was supported by the projects GACR 14-12449S and VEGA 1/0182/16.

References

[1] M. F. Ashby, A. L. Greer. *Scripta Mater.* **54**, 321 (2006).
[2] A. Inoue, A. Takeuchi. *Acta Mater.* **59**, 2243 (2011).
[3] G. Herzer. *Acta Mater.* **61**, 718 (2013).
[4] Ch. A. Schuh, T. C. Hufnagel, U. Ramamurty. *Acta Mater*, **55**, 4067 (2007).
[5] M. E. McHenry, D. E. Laughlin. *Acta Mater.* **48**, 223 (2000).
[6] K. Suzuki, G. Herzer. *Scripta Mater.* **67**, 548 (2012).
[7] Y. Yoshizawa, A. Oguma, K. Yamauchi. *J. Appl. Phys.* **64**, 6044 (1988).
[8] K. Suzuki, N. Kataoka, A. Inoue, A. Makino, T. Masumoto. *Mater. Trans. JIM.* **31**, 743 (1990).
[9] M. A. Willard, D. E. Laughlin, M. E. McHenry, D. Thoma, K. Sickafus, J. O. Cross, V. G. Harris. *J. Appl. Phys.* **84**, 6773 (1998).
[10] A. Makino, H. Men, T. Kubota, K. Yubuta, A. Inoue. *J. Appl. Phys.* **105**, 07A308 (2009).
[11] R. Hasegawa. *J. Magn. Magn. Mater.* **324**, 3555 (2012).
[12] Ph. Gütlich, E. Bill, A. X. Trautwein. *Mössbauer Spectroscopy and Transition Metal Chemistry*. Springer, Heilderberg Dordrecht London New York (2011).
[13] M. Miglierini, J.-M. Grenèche. *J. Phys. Condens. Matter.* **9**, 2303 (1997).
[14] M. Miglierini, J.-M. Grenèche. *J. Phys. Condens. Matter.*, **15**, 5637 (2003).
[15] G. Mülhaupt, R. Rüffer. *Hyperfine Int.* **123/124**, 13 (1999).
[16] N. Mattern, M. Stoica, G. Vaughan, J. Eckert. *Acta Mater.* **60**, 517 (2012).
[17] G. Wang, N. Mattern, J. Bednarčík, R. Li, B. Zhang, J. Eckert. *Acta Mater.* **60**, 3074 (2012).

[18] T. Egami, Y. Tong, W. Dmowski. *Metals*. **6**, 22 (2016).
[19] C. Puncreobutr, A. B. Phillion, J. L. Fife, P. Rockett, A. P. Horsfield, P. D. Lee. *Acta Mater.* **79**, 292 (2014).
[20] V. M. Giordano, B. Ruta. *Nature Comm.* **7**, 10344 (2016).
[21] G. V. Smirnov. *Hyperfine Int.* **123**/**124**, 31 (1999).
[22] M. Miglierini, V. Prochazka, S. Stankov, P. Svec Sr., M. Zajac, J. Kohout, A. Lancok, D. Janickovic, P. Svec. *Phys Rev B.* **86**, 020202(R) (2012).
[23] M. Miglierini, V. Procházka, R. Rüffer, R Zbořil. *Acta Mater.* **91**, 50 (2015).
[24] V. Procházka, V. Vrba, D. Smrčka, R. Rüffer, P. Matúš, M. Mašláň, M. Miglierini. *J Alloy Compounds*. **638**, 398 (2015).
[25] M. Miglierini, M. Pavlovič, V. Procházka, T. Hatala, G. Schumacher, R. Rüffer. *Phys. Chem. Chem. Phys.* **17**, 28239 (2015).
[26] R. Röhlsberger. *Nuclear Condensed Matter Physics with Synchrotron Radiation*. Springer-Verlag, Berlin Heidelberg (2004).
[27] M. Seto. *J. Phys. Soc. Jpn*. **82**, 021016 (2013).
[28] R. Rüffer. *C. R. Physique*. **9**, 595 (2008).
[29] T. Žák, Y. Jirásková. *Surf. Interf. Anal.* **38**, 710 (2006).
[30] W. Sturhahn. E. Gerdau. *Phys. Rev. B* **49**, 9285 (1994).
[31] W. Sturhahn. *Hyperfine Interact.* **125**, 149 (2000).
[32] V. Vrba, V. Procházka, D. Smrčka, M. Miglierini. in: AIP Conference Proceedings 1781, 020013 (2016).
[33] V. Vrba, V. Procházka, D. Smrčka, M. Miglierini. *Nucl. Inst. Meth. Phys. Res. A* **847**, 111 (2017).